NUKLEONIKA 2007;52(Supplement 1):S37–S41

Mössbauer studies of structure relaxations near nanocrystallization region in amorphous $Fe_{90}Zr_7B_3$ alloy

Jan Świerczek, Józef Lelątko

Abstract. Transmission Mössbauer spectra and high-resolution electron microscopy investigations for amorphous $Fe_{90}Zr_7B_3$ alloy in the as-quenched state and after annealing in vacuum at temperatures 673, 723 and 743 K have been performed. In the as-quenched state the microstructure reveals the presence of medium range order BCC- or FCC-like structure regions 1–3 nm in size which grow during annealing at 673 K being the nuclei of grains of α-Fe phase. After annealing at 723 K for 1 h, the grains 16 nm in diameter and with the average distance of 110 nm between them are embedded in the paramagnetic amorphous matrix. This distance is large enough to prevent magnetic interaction between the grains, and superparamagnetic behavior is observed. After longer annealing at 723 K and at 743 K, the Mössbauer spectra show a crystalline component of the α-Fe phase with the inhomogeneous amorphous matrix consisting of para- and ferromagnetic phases. The hyperfine induction of the crystalline phase slightly increases with time and annealing temperature which is ascribed to the faster diffusion of atoms.

Key words: amorphous structure relaxation • nanocrystallization • Mössbauer spectroscopy

J. Świerczek✉
Institute of Physics,
Częstochowa University of Technology,
19 Armii Krajowej Ave., 42-200 Częstochowa, Poland,
Tel.: +48 34 3250791, Fax: +48 34 3250795,
E-mail: swiercz@mim.pcz.czest.pl

J. Lelątko
Institute of Materials Science,
University of Silesia,
12 Bankowa Str., 40-007 Katowice, Poland

Received: 20 June 2006
Accepted: 30 November 2006

Introduction

From the thermodynamic point of view, amorphous structure is not stable and during annealing tends through metastable states towards crystalline state. Due to the lack of long range atom ordering, the structure changes involve topological short range order (TSRO) and chemical short range order (CSRO) of atoms. The changes in TSRO and CSRO are called structure relaxations [2]. Mössbauer spectroscopy is a powerful tool for these relaxations studies because hyperfine interactions, especially quadrupole splitting (QS), are sensitive to the local environment.

The amorphous $Fe_{90}Zr_7B_3$ alloy is a precursor of NANOPERM-type nanocrystalline material obtained by the conventional annealing [13]. The Curie temperature of this alloy is below room temperature, so at and above the ambient temperature quadrupole interaction is not hidden by the much stronger magnetic one. For this reason, the material is a good candidate for structure relaxations studies in the amorphous state. The amorphous $Fe_{90}Zr_7B_3$ alloy crystallizes in two stages [8]. At the first stage, the α-Fe precipitations occur in the residual amorphous matrix, and at the second, the crystallization of the matrix takes place. When the volume fraction of the crystalline phase after primary crystallization is about 0.6–0.7, owing to the averaging out of the magnetic anisotropy, the material exhibits excellent soft magnetic properties, i.e. low coercivity, high magnetic permeability and high saturation magnetization, provided that the residual amorphous phase is in the ferromag-

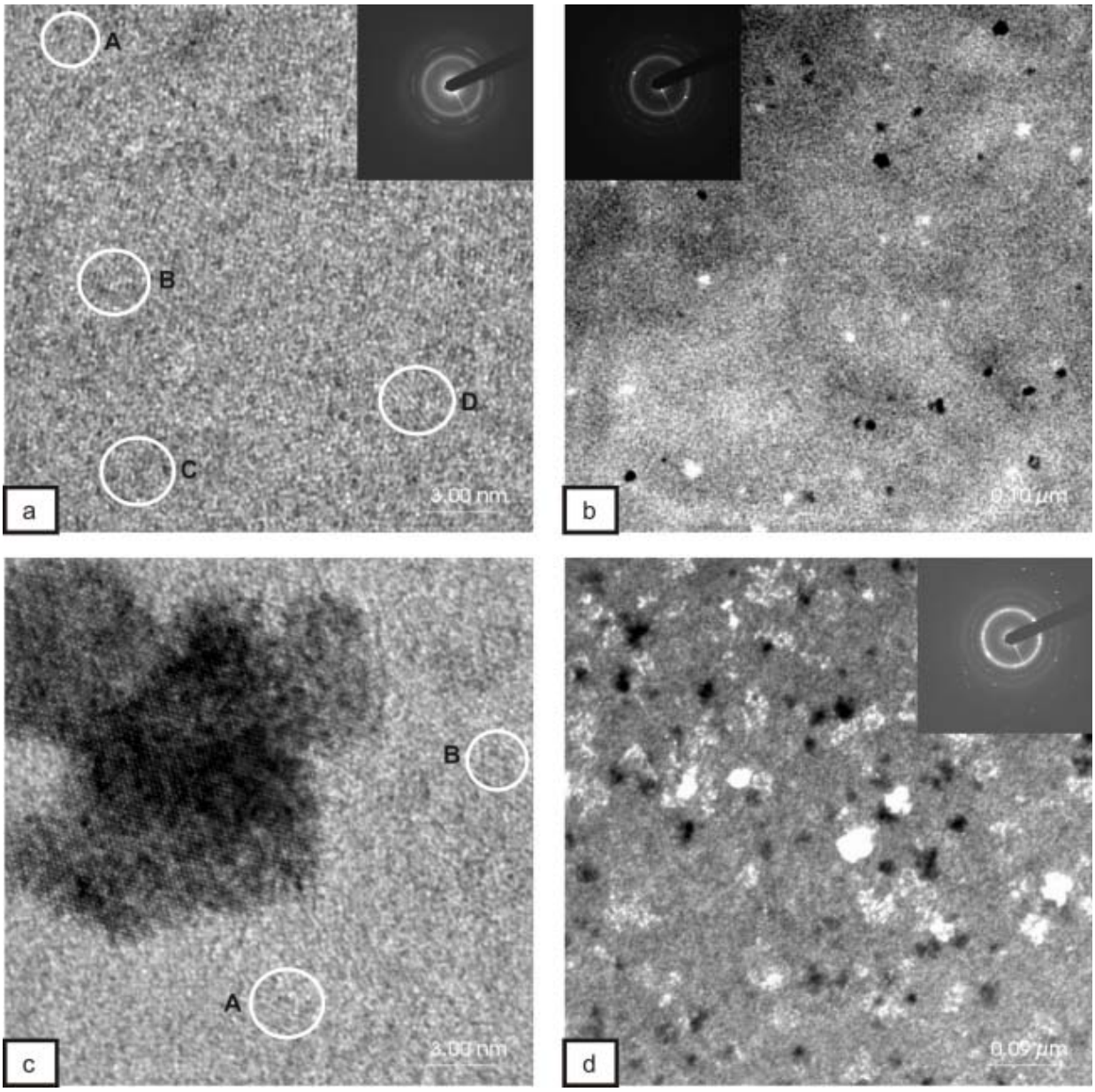

Fig. 1. Transmission electron microscope images for the amorphous $Fe_{90}Zr_7B_3$ alloy: (a) as-quenched state, (b, c) after annealing at T_{a2} = 723 K for 1 h and (d) after annealing at T_{a2} = 723 K for 2 h. Selected area diffraction patterns are shown as insets.

netic state. The soft magnetic properties deteriorate drastically at temperatures higher than the Curie point of the amorphous matrix [5]. For alloys containing Fe atoms, Mössbauer spectroscopy is a very useful method for qualitative and quantitative phase analyses in nanocrystalline materials [3, 6]. Ohkubo *et al*. [10] performed studies of structural changes during the primary crystallization of the amorphous $Fe_{90}Zr_7B_3$ alloy by means of modern electron microscope techniques, and proposed the model for local structure changes of $Fe_{90}Zr_7B_3$ alloy during annealing. They observed the existence of the BCC-like medium range order (MRO) regions in the as-quenched state and their growth during annealing, being the nuclei of α-Fe grains in the primary crystallization.

In this paper, we have used Mössbauer spectroscopy to investigate structure relaxations in the amorphous $Fe_{90}Zr_7B_3$ alloy, subjected to annealing at 3 different temperatures; below and above the onset of the primary crystallization. For the same stages of annealing, the high-resolution electron microscopy (HREM) observations have been performed.

Experimental procedure

Amorphous $Fe_{90}Zr_7B_3$ alloy ribbons were prepared by the melt spinning method. The ribbons were about 20 μm thick and 1.5 cm wide. The square specimens 1.5 × 1.5 cm^2 were subjected to the accumulative annealing in vacuum of 1.33×10^{-3} Pa at 3 temperatures: T_{a1} = 673 K, T_{a2} = 723 K and T_{a3} = 743 K. According to the DSC results reported in [8], the first annealing temperature is below the start of the primary crystalli-

zation and only relaxations within the amorphous state are expected. The second is the onset of the primary crystallization, and the third lies in the primary crystallization range. At each stage of heat treatment, the transmission Mössbauer spectra were recorded at room temperature for all samples by means of a conventional constant acceleration spectrometer with a ^{57}Co(Rh) source. The spectrometer was calibrated and the isomer shift (IS) was determined with respect to the α-Fe polycrystalline foil. To improve the resolution, the spectra for specimens exhibiting only quadrupole splitting were recorded also at narrow velocity range. Fittings were carried out by NORMOS package written by Brand [1]. The microstructure of the samples and its changes after each annealing were observed by high-resolution electron microscopy. A JEM 3010 microscope was used.

Results and discussion

In Fig. 1 the high-resolution electron microscope images and the corresponding electron diffraction patterns of the selected areas, as insets, for the amorphous $Fe_{90}Zr_7B_3$ alloy in the as-quenched state and after annealing for 1 and 2 h at T_{a2} = 723 K are shown. In the as-quenched state the microstructure and electron diffraction pattern are typical of the amorphous state, although in the encircled areas fringe like structure ascribed to MRO regions with a size of 1–3 nm are visible (Fig. 1a). After annealing at T_{a2} = 723 K for 1 h, the crystalline grains of α-Fe phase appear in the amorphous matrix (Fig. 1b). The average size of the grains is about 16 nm and the average distance between the boundaries of the adjacent grains is about 110 nm. HREM image, showed in Fig. 1c, indicates that the grains are not regular in shape and MRO regions are also presented in the residual amorphous matrix. After heat treatment for 2 h at the same temperature (Fig. 1d) the mean size of the α-Fe grains remains the same (16 nm) with the average distance of 40 nm between them.

The transmission Mössbauer spectra for the amorphous $Fe_{90}Zr_7B_3$ alloy in the as-quenched state and after accumulative annealing at T_{a1} = 673 K are depicted in Fig. 2A. Typical of amorphous paramagnetic material spectra are asymmetric indicating correlation between IS and QS. The distributions P(QS), shown in Fig. 2B, are obtained assuming a linear correlation between IS and QS. It is worth noticing that the P(QS) distributions exhibit three characteristic points; not vanishing probability for QS = 0 and two local maxima, P_1 and P_2 (Fig. 2B). Non-zero probability $P_0 = P(QS)=0$ means that there are Fe sites in the amorphous structure with cubic symmetry of atom arrangement in the nearest neighborhood. These Fe sites may be attributed to the MRO domains (Fig. 1). Two local maxima P_1 and P_2 of P(QS) distribution correspond to the Fe sites having only Fe atoms with local symmetry lower than cubic in atom arrangement and Fe and Zr atoms in the nearest neighborhood, respectively. The probability of P_0 increases, whereas P_1 and P_2 decrease with time of annealing at T_{a1} = 673 K (Fig. 3). According to P(QS) distributions, the spectra shown in Fig. 2A, can be decomposed into three subspectra: two quadrupole doublets and a single line. Such a decomposition for the sample in the as-quenched state is presented in Fig. 4 as an example. The quadrupole splittings of the

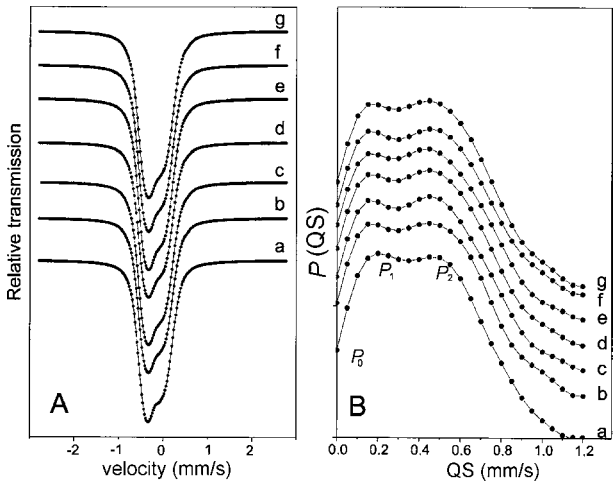

Fig. 2. Transmission Mössbauer spectra (A) and corresponding P(QS) distributions (B) for the amorphous $Fe_{90}Zr_7B_3$ alloy in the as-quenched state (a) and after annealing at T_{a1} = 673 K for: 1 h (b), 2 h (c), 3 h (d), 4 h (e), 5 h (f) and 6 h (g). Characteristic points of the P(QS) distributions are denoted as P_0, P_1 and P_2.

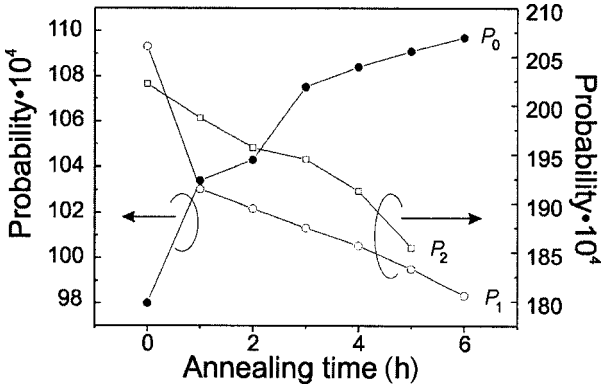

Fig. 3. The probability P_0, P_1 and P_2 vs. the annealing time at T_{a1} = 673 K for the amorphous $Fe_{90}Zr_7B_3$ alloy.

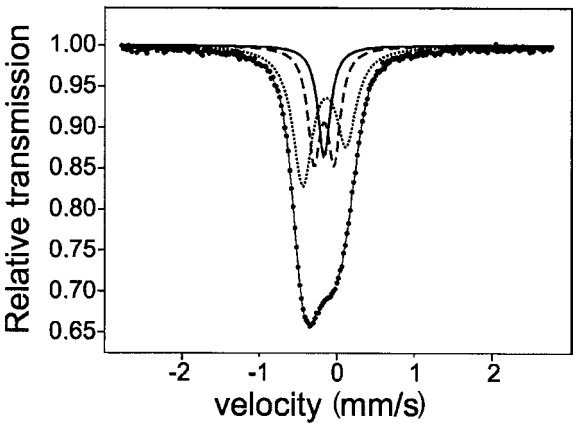

Fig. 4. Decomposition of the Mössbauer spectrum for the amorphous $Fe_{90}Zr_7B_3$ alloy in the as-quenched into two quadrupole doublets (dashed and dotted lines) and a single line (solid).

doublets are equal to $QS_1 = 0.26 \pm 0.01$ mm/s and $QS_2 = 0.57 \pm 0.01$ mm/s and remain, within the experimental error, almost unchanged after annealing at $T_{a1} = 673$ K. The best fitting is obtained assuming the fixed values of the half widths of the first doublet and the singlet to be 0.194 mm/s, whereas the half width of the second doublet is fitted and amounts to 0.311 ± 0.001 mm/s. The isomer shift of the single-line component is equal to $IS = -(0.06 \pm 0.003)$ mm/s and the area increases from 18% to 24% of the whole spectrum area at the expense of the doublet areas which decrease after annealing at $T_{a1} = 673$ K. It means that MRO domains, understood as an assembly of Fe sites with cubic symmetry of Fe atoms arrangement, grow in the course of annealing at $T_{a1} = 673$ K. As mentioned above, Ohkubo *et al*. claim, basing only on modern electron microscope observations [10] that the MRO regions are BCC-like Fe structure and growing during annealing become the nuclei of α-Fe crystalline phase. On the other hand, Fernández-Gubieda *et al*. report, using the EXAFS method [4] that the average Fe-Fe coordination number in the amorphous $Fe_{91}Zr_7B_2$ alloy is higher than 11. Taking into account that the coordination number of the α-Fe phase with FCC structure is equal to 12 and the isomer shift to –0.09 mm/s [7], one can believe that the MRO regions are not only BCC-like but FCC-like Fe structure, as well. So, crystallization takes place not only by simple growth of the BCC-like Fe structure but also by more collective process of atom arrangements involving FCC-BCC transformation, because the product of the primary crystallization is mainly α-Fe phase [10].

The transmission Mössbauer spectra for the amorphous $Fe_{90}Zr_7B_3$ alloy in the as-quenched state and after accumulative annealing at $T_{a2} = 723$ K for 1–5 h and at $T_{a3} = 743$ K for 1–3 h are depicted in Figs. 5A and 5B. After annealing at $T_{a2} = 723$ K for 1 h, the spectrum does not show the crystalline component (Fig. 5Ab), whereas the micrograph reveals the presence of α-Fe grains in the amorphous matrix (Fig. 1b). The critical diameter for a single magnetic domain of α-Fe particles is about 50 nm [9]. The α-Fe grains of 16 nm in average size can be treated as single domain particles embedded in paramagnetic amorphous matrix. Because the distance between the adjacent grains is large enough (110 nm) to prevent magnetic interaction, they behave like superparamagnetic particles. The reciprocal of the superparamagnetic relaxation time is higher than the nuclear Larmor precession frequency, so the effective magnetic field at Fe nuclei is averaged out to zero and, consequently, the sextet in the Mössbauer spectrum is not present (Fig. 5Ab). When the annealing time is 1 h longer, the average grain size remains the same but the distance between them decreases leading to the occurrence of magnetic dipolar interaction between grains and the spectrum shows the α-Fe component (Fig. 5Ac). In this case the prolongation of the superparamagnetic relaxation time for some grains may not be excluded. The spectra, which exhibit the α-Fe sextet, were fitted using one crystalline component and two distributions of the quadrupole splitting in paramagnetic and hyperfine induction in ferromagnetic phase of the amorphous matrix. The last phase contains also atoms

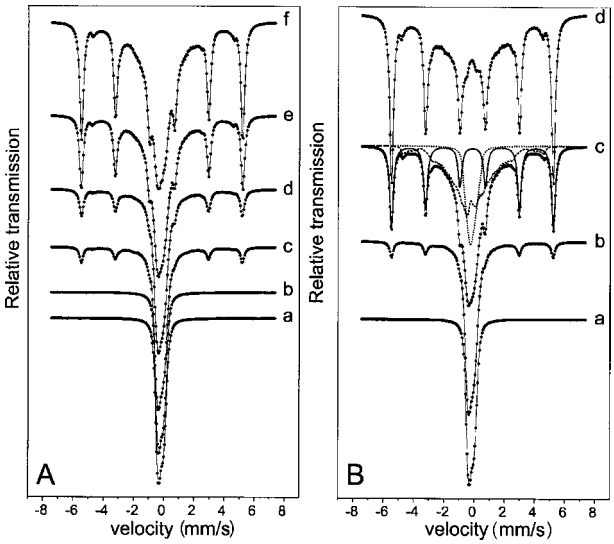

Fig. 5. Mössbauer spectra for the amorphous $Fe_{90}Zr_7B_3$ alloy in the as-quenched state (a) and subjected to annealing at $T_{a2} = 723$ K (A) and $T_{a3} = 743$ K (B) for: 1 h (b), 2 h (c), 3 h (d), 4 h (e) and 5 h (f). An example fitting is depicted for the sample annealed at $T_{a3} = 743$ K for 2 h. Solid line – crystalline component, dashed line – ferromagnetic phase and dotted line – paramagnetic phase of the amorphous matrix.

lying in the interface [11]. This kind of fitting is presented in Fig. 5Bc, as an example. Figure 5Bd shows that the amorphous matrix of the sample annealed at $T_{a3} = 743$ K for 3 h does not reveal the paramagnetic phase. In Table 1 are listed: the value of the hyperfine induction, B_{cr}, the isomer shift, IS_{cr}, volume fraction, x for the crystalline α-Fe phase, the average value of the quadrupole splitting, QS_{av}, its standard deviation, ΔQS, in paramagnetic and the average hyperfine induction, B_{av}, its standard deviation, ΔB_{hf}, in ferromagnetic phase of the amorphous matrix for the $Fe_{90}Zr_7B_3$ amorphous alloy in the as-quenched state and after annealing at $T_{a2} = 723$ K and $T_{a3} = 743$ K. As can be seen from Table 1, the hyperfine induction of the α-Fe phase, B_{cr}, slightly increases with time and annealing temperature. It is due to the fact that the Zr atom diffusion out of the crystalline grains is faster at higher annealing temperature. It is worth noticing that the volume fraction of α-Fe phase also increases with time and annealing temperature (Table 1). The appearance of the crystalline phase effects the short range order in residual amorphous matrix, which becomes more inhomogeneous, because ΔQS and ΔB in the amorphous matrix increase with time and annealing temperature (Table 1). The regions close to the grains are poorer in Fe atoms than the parent alloy and they are coupled ferromagnetic giving rise to the ferromagnetic phase within the amorphous matrix. The average hyperfine induction of the ferromagnetic phase in the amorphous matrix, B_{av}, also increases, because the higher the volume fraction of the crystalline phase the lower Fe atoms concentration in the matrix which are ferromagnetic coupled. The Curie temperature of this phase may additionally be enhanced due to exchange interaction penetration from a grain via the interface to the matrix [11, 12]. The satellite sharp lines visible in Figs. 5Ae, 5Af, 5Bc and

Table 1. The values are listed of the hyperfine induction, B_{cr}, isomer shift, IS_{cr}, volume fraction, x for the crystalline α-Fe phase, average value of the quadrupole splitting, QS_{av}, its standard deviation, ΔQS, in paramagnetic and the average hyperfine induction, B_{av}, its standard deviation, ΔB, in ferromagnetic phase of the amorphous matrix for the $Fe_{90}Zr_7B_3$ amorphous alloy in the as-quenched state and after annealing at T_{a2} = 723 K and T_{a3} = 743 K. Uncertainties for the last significant figure are given in brackets

Thermal history of the sample	B_{cr} (T)	IS_{cr} (mm/s)	x (%)	QS_{av} (mm/s)	ΔQS (mm/s)	B_{av} (T)	ΔB (T)
As-quenched	–	–	–	0.412(1)	0.260(1)	–	–
723 K/1 h	–	–	–	0.428(1)	0.274(1)	–	–
723 K/2 h	32.99(1)	–0.029(1)	39(1)	0.444(1)	0.294(1)	9.07(1)	7.67(1)
723 K/3 h	33.03(1)	–0.027(1)	46(1)	0.451(1)	0.298(1)	9.45(1)	7.76(1)
723 K/4 h	33.06(1)	–0.025(1)	51(1)	0.454(1)	0.309(1)	9.79(1)	7.86(1)
723 K/5 h	33.14(1)	–0.026(1)	56(1)	0.600(1)	0.334(1)	10.66(1)	7.99(1)
743 K/1 h	33.08(1)	–0.027(1)	38(1)	0.432(1)	0.281(1)	9.88(1)	7.28(1)
743 K/2 h	33.11(1)	–0.026(1)	52(1)	0.484(1)	0.335(1)	10.76(1)	7.62(1)
743 K/3 h	33.13(1)	–0.027(1)	65(1)	–	–	14.28(1)	7.96(1)

5Bd correspond to the component with the hyperfine field about 29 T which is ascribed to the interface [11] because other crystalline phases (for example borides) are not detected by electron microscope.

Conclusions

- The amorphous $Fe_{90}Zr_7B_3$ alloy subjected to accumulative annealing for 6 h at T_{a1} = 673 K does not show crystallization. The structure relaxations within the amorphous state lead to the growth of the MRO regions which may exhibit BCC- or FCC-like structure and become the nuclei of crystalline phase.
- After annealing of the amorphous $Fe_{90}Zr_7B_3$ alloy for 1 h at T_{a2} = 723 K, the average size of the crystalline grains and the average distance between them are about 16 nm and 110 nm, respectively. The Mössbauer spectrum does not reveal the crystalline component due to superparamagnetic relaxation effect.
- The hyperfine induction of the crystalline α-Fe phase slightly increases with time and annealing temperature, owing to the Zr atoms diffusion out of the grains.
- After annealing at T_{a2} = 723 K and T_{a3} = 743 K, the amorphous matrix consists of two phases; paramagnetic and ferromagnetic. The inhomogeneity of the matrix increases with time of annealing at both temperatures.

Acknowledgments The authors thank Dr A. Makino from Central Research Laboratory, Alps Electronic Corporation (Japan) for kindly supplying the ribbon.

References

1. Brand RA (1987) Improving the validity of hyperfine field distributions from magnetic alloys. Nucl Instrum Methods Phys Res B 28:398–416
2. Brüning R, Altounian Z, Ström-Olsen JO (1987) Reversible structural relaxation in Fe-Ni-B-Si metallic glasses. J Appl Phys 62:3633–3638
3. Brzózka K, Ślawska-Waniewska A, Nowicki P, Jezuita K (1997) Hyperfine magnetic fields in FeZrB(Cu) alloys. Mater Sci Eng A 226/228:654–658
4. Fernández-Gubieda ML, Gorria P, Barandiarán JM, Fernandez Barquín L (1995) EXAFS study of short range order in Fe-Zr amorphous alloys. Nucl Instrum Methods Phys Res B 97:206–208
5. Garitaonandia JS, Schmool DS, Barandiarán JM (1998) Model of exchange-field penetration in nanocrystalline $Fe_{87}Zr_6B_6Cu$ alloys from magnetic and Mössbauer studies. Phys Rev B 58:12147–12158
6. Grenèche JM, Miglierini M, Ślawska-Waniewska A (2000) Iron-based nanocrystalline alloys investigated by ^{57}Fe Mössbauer spectroscopy. Hyperfine Interact 126:27–34
7. Kopcewicz M, Grabias A, Nowicki P, Williamson DL (1996) Mössbauer and x-ray study of the structure and magnetic properties of amorphous and nanocrystalline $Fe_{81}Zr_7B_{12}$ and $Fe_{79}Zr_7B_{12}Cu_2$ alloys. J Appl Phys 79:993–1003
8. Makino A, Inoue A, Masumoto T (1995) Nanocrystalline soft magnetic Fe-M-B (M=Zr, Hf, Nb) alloys produced by crystallization of amorphous phase. Mater Trans JIM 36:924–938
9. O'Handley RC (2000) Modern magnetic materials. Principles and applications. John Wiley and Sons, New York
10. Ohkubo T, Kai H, Makino A, Hirotsu Y (2001) Structural change of amorphous $Fe_{90}Zr_7B_3$ alloy in the primary crystallization process studied by modern electron microscope techniques. Mater Sci Eng A 312:274–283
11. Ślawska-Waniewska A, Grenèche JM (1997) Magnetic interfaces in Fe-based nanocrystalline alloys determined by Mössbauer spectroscopy. Phys Rev B 56:R8491–R8494
12. Suzuki K, Cadogan JM (2000) Effect of Fe-exchange-field penetration on the residual amorphous phase in nanocrystalline $Fe_{92}Zr_8$. J Appl Phys 87:7097–7099
13. Suzuki K, Makino A, Inoue A, Masumoto T (1993) Low core losses of nanocrystalline Fe-M-B (M = Zr, Hf or Nb) alloys. J Appl Phys 74:3316–3322